Thermal energy harvesting from the human body using flexible thermoelectric generator (FTEG) fabricated by a dispenser printing technique

CrossMark

Abu Raihan Mohammad Siddique, Ronil Rabari, Shohel Mahmud*, Bill Van Heyst

School of Engineering, University of Guelph, Ontario, Canada

ABSTRACT

In this paper, a manual dispenser printing-based fabrication technique has been developed to synthesize a flexible thermoelectric generator (FTEG). Fabricated FTEGs, printed on polyester fiber clothe, convert the thermal energy from the human body into electrical energy using the Seebeck effect. Two flexible prototypes (prototype A and prototype B) were fabricated using a manual dispenser printing technique with *n*-type $(0.98Bi,0.02Sb)_2(0.9Te,0.1Se)_3$ and *p*-type $(0.25Bi,0.75Sb)_2(0.95Te,0.05Se)_3$ thermoelectric (TE) materials. The fabricated prototypes consisted of 12 pairs of *n*-type and *p*-type legs connected by silver conductive threads. The experimental investigations were conducted to determine the characteristics and the electrical outputs of the fabricated prototypes. The open circuit voltage and power output of prototype A and prototype B were 22.1 mV and 2.21 nW, and 23.9 mV and 3.107 nW, respectively, at 22.5 °C temperature difference. The fabricated prototypes were also tested on the human body at different body conditions and were found to be very flexible, twistable, and durable with the substrate as well as conforming well to the human body.

© 2016 Elsevier Ltd. All rights reserved.

1. Introduction

Microelectromechanical systems (MEMS) have made self-powered portable electronic devices (e.g., tracking devices [1], biosensors [2], smart wrist watches, hearing aids, and Google glasses [3]) more practical and convenient in terms of power consumption. Over the last two decades, developments in MEMS and the miniaturization of electronic devices have reduced the power demand in the range of mW to μW level for the wireless sensor network (WSN) [4,5]. This small amount of power requirement is usually fulfilled by traditional electrochemical batteries [6,7]. However, the traditional batteries need to be changed on a regular basis and are toxic to the environment [8,9]. Thermoelectric (TE) power harvesting using thermal energy from the human body can be one of the attractive alternative solutions to conventional batteries. The environmentally friendly thermoelectric generator (TEG) is a solid state compact device that can convert thermal energy into electrical energy using a single step of energy conversion [10,11]. TEGs are capable of harvesting energy from waste and low

exergy renewable thermal energy sources; for example, solar heat, thermal energy from the human body, and any other kind of waste heat from machinery. TEGs have many advantages over many traditional small-scale power generation systems in that they are compact, easy to fabricate, easy to conform to the human body, less costly to implement, silent in operation, have longer operational time, and it has no moving parts [12,13]. Therefore, such characteristics of TEGs make them environmentally friendly. In order to have the best use of the TEG on the human body for energy harvesting, it should be wearable and flexible. Recent advancement in the small scale TE system manufacturing techniques makes flexible TEG (FTEG) more advantageous for self-powered portable electronic devices.

Since 2001, FTEG has been a very active research area using different fabrication techniques [14]. These fabrication techniques include dispenser printing [15], evaporation [16], lift off process [17], lithography and etching [18], screen printing [19], and sputtering [20]. Yadav et al. [16] used a thin film evaporative technique to fabricate the FTEG prototype with Nickel-Silver (Ni−Ag) materials of 7 pairs of *n*-type and *p*-type TE legs with a power output of 2 nW at a temperature difference of 6.6 K. Hasebe et al. [17] designed a FTEG using lift-off process with Nickel-Copper

---

* Corresponding author.
 E-mail address: smahmud@uoguelph.ca (S. Mahmud).

Nomenclature

a	Length of the TE leg (mm)
A	Cross sectional area of TE leg (mm^2)
b	Width of the TE leg (mm)
h	Heat transfer coefficient (Wm^{-2} K^{-1})
I_L	Electrical load current (A)
K	Thermal conductance (W °C^{-1})
k	Thermal conductivity (Wm^{-1} °C^{-1})
l	Thickness or height of the TE leg (mm)
n	Number of TE legs
P	Instantaneous power output (W)
$\dot{Q}_H$	Rate of heat entering to the hot side of the TE system (W)
$\dot{Q}_C$	Rate of heat leaving from the cold side of the TE system (W)
R_{in}	Internal electrical resistance (Ω)
R_L	Load resistance (Ω)
T_H	Hot body temperature (°C)
T_{Hs}	Hot surface temperature of FTEG (°C)
T_C	Cold side temperature (°C)
T_{Cs}	Cold surface temperature of FTEG (°C)
ΔT	Temperature difference between hot side and ambient (°C)
ΔT_{TEG}	Temperature difference between FTEG surfaces (°C)
U_p	Relative uncertainty of output power
U_V	Accuracy of the measuring instrument for voltage
U_I	Accuracy of the measuring instrument for current
V	Electric potential (V)
x_V	Measured value of voltage by multimeter
x_I	Measured value of current by multimeter

Greek letters

α	Seebeck coefficient (μVK^{-1})
ρ	Electrical resistivity (Ωm)

Subscripts

TEG	Thermoelectric generator
C	Cold
Cs	Cold surface of FTEG
H	Hot body
Hs	Hot surface of FTEG
I	Current
in	Internal
L	Load
max	Maximum
n	n-type TE material/leg
P	Power
p	p-type TE material/leg
V	Voltage

(Ni–Cu) on polyimide sheet which had a voltage output of 15.4 μVK^{-1} using 78 couples of n-type and p-type TE legs. Francioso et al. [20] used Radio Frequency-magnetron (RF) co-sputtering method for integrating 100 TE couples for their FTEG prototype with a generated power output of 4 nW at 15 K. Navone et al. [19] and Suemori et al. [21] used screen printing technology for fabricating an FTEG with 5 and 108 pairs of n-type (Bismuth-Selenium-Telluride) Bi$_2$Se$_{0.3}$Te$_{2.7}$ and p-type (Bismuth-Antimony-Telluride) Bi$_{0.5}$Sb$_{1.5}$Te$_3$, carbon nanotubes and polystyrene material, respectively, on the polyethylene naphthalate (PEN) substrate. The power density of the fabricated prototype was 55 mWm^{-2}[21].

Most of the printing fabrication techniques (e.g., chemical vapor deposition, lithography and etching, screen printing, sputtering, etc.) are complex and expensive which require very high curing temperature (300–600 °C) and highly configured electronic equipment during fabrication (e.g., controlled dispenser, hot press machine, printed circuit board, sputtering machine, thin film etc.) [15–21]. In contrast, the dispenser printing techniques are relatively simple, less expensive, and it does not require any thin film mechanism. Moreover, it requires low curing temperatures in the range of 100–200 °C. Recently, the dispenser printing technique has been used for fabricating FTEGs for various applications [15], [22–24]. Jo et al. [15] fabricated a FTEG prototype with 8 TE couples of n-type and p-type Bi$_2$Te$_3$ on polydimethylsiloxane (PDMS) thick substrate. The power output of their prototype was 2.1 μW at 19 K. Madan et al. [22] using similar technology developed an FTEG with an epoxy composite thin film by integrating 60 TE elements which had a power output of 20.5 μW at 20 K. More recently, Kim et al. [23,24] used 12 and 20 pairs of n-type and p-type Bi$_2$Te$_3$, respectively, on polymer fabric as a substrate to fabricate FTEG prototype. A maximum power output of 178 nW at 27 K [23] and 224 nW at 15 K [24] was measured from their designed FTEG prototypes.

From the literature reviewed on the dispenser printing fabrication technique, it is apparent that the reported dispenser printing techniques are still a costly and complex process [19,25] for widespread practical use due to the requirement of appropriate substrates (e.g., high heat resistive, thin, and flexible substrates), controlled dispensing equipment, and high curing temperature. In the current research, a simple and easy way to conduct the dispenser printing technique compared to other dispenser printing techniques has been demonstrated to fabricate FTEGs. The complete fabrication process, except the curing step, is performed manually (e.g., preparing substrate, sewing process to connect n-leg and p-leg, filling up the holes with TE paste). This fabrication technique provides wearability and flexibility to FTEG for thermal energy harvesting from the human body. The FTEG comprises of polyester fabric, silver thread, n-type and p-type bismuth telluride powder, liquid binder, and Kapton thin film for insulation between the TEG and the skin.

2. Flexible thermoelectric generator

Typically, a TEG is a solid-state heat engine which consists of a number of n-type and p-type TE legs. TE legs are interconnected with conductive wires and covered with thermally conductive but electrically insulated rigid substrates at the top and bottom surfaces. A TEG can be referred to as a FTEG when the rigid substrate is replaced by a flexible substrate (e.g., thin film, fabric clothes etc.). FTEGs are compliant to curved surfaces such as human body. Fig. 1 schematically represents the magnified version of a unit cell of a FTEG.

A typical FTEG is made up of multiple unit cells similar to Fig. 1. These cells are connected electrically in series and thermally in parallel. According to the Seebeck effect, an electric potential is established when two dissimilar TE materials are connected together with an applied temperature difference across the junctions [26]. The generated electric potential is directly proportional to the temperature gradient between the hot and cold surfaces of the FTEG which can be expressed as:
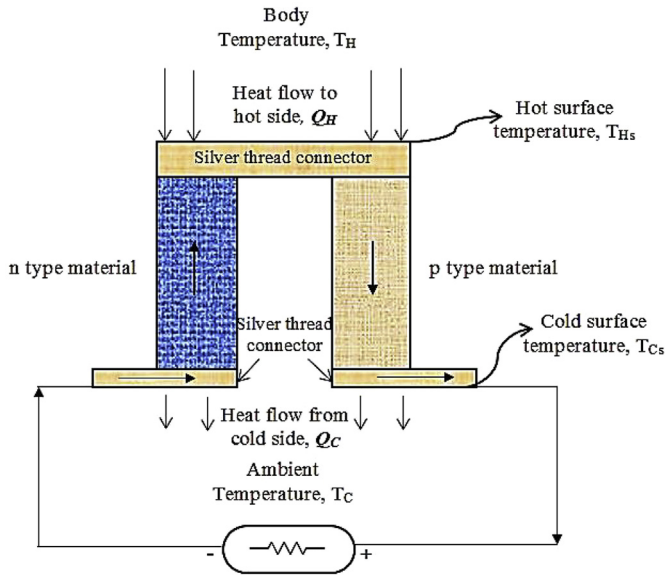
Fig. 1. Schematic diagram of a single thermoelectric cell.

$$V = n\alpha\Delta T_{TEG} \qquad (1)$$

where, V is the electric potential, n is the number of TE legs, α is the Seebeck coefficient, and ΔT_{TEG} is the temperature difference across the FTEG surfaces. The instantaneous power (P) harvested by FTEG can be calculated as:

$$P = VI_L \qquad (2)$$

$$P = \frac{V^2}{(R_L + R_{in})^2} \times R_L \qquad (3)$$

where, I_L is the electrical load current output, R_L is the load resistance, and R_{in} is the internal resistance of the TE legs. Equation (3) shows that power output increase with decreasing internal resistance value and vice versa [23]. Therefore, R_{in}, which depends on the thickness of the TE legs, plays an important role in power generation. Moreover, the voltage output of the FTEG depends on the temperature gradient, TE materials properties (i.e., Seebeck coefficient, thermal conductivity, and electrical conductivity), and the geometric design of the legs [27–29].

Flexibility is an important criterion of an FTEG to harvest thermal energy from the human body due to the curved surfaces encountered. In order to make an FTEG, it is very important to select a proper flexible substrate which can provide elasticity to the substrate. A schematic diagram of a FTEG is shown in Fig. 2.
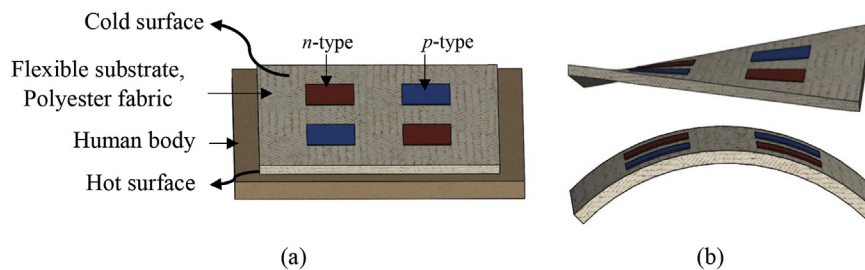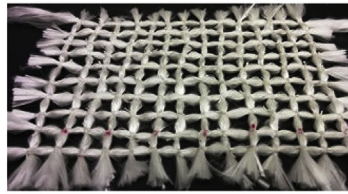
3. Materials specifications and fabrication steps

3.1. Material specifications

The FTEG prototypes include a substrate, n-type and p-type TE materials, an adhesive binder material, Kapton film, and silver thread to connect TE legs. The substrate of the prototypes consist of polyester based fabric (supplier: A-B Thermal Technologies) which can withstand temperature up to 593 °C. The n-type $(0.98Bi,0.02Sb)_2(0.9Te,0.1Se)_3$ powder and p-type $(0.25Bi,0.75Sb)_2(0.95Te,0.05Se)_3$ powder are used as TE materials (supplier: Hi-Z Technology Inc.). TE powder materials are mixed with an adhesive binder (Durabond-950, supplier: iS-Connect) which is a combination of powder and the liquid thinner refractory ceramic colloid. Silver connective thread with an electrical resistance of 0.65 Ωcm^{-1} (supplier: Lame lifesaver) is used to connect n-type and p-type TE legs. Additionally, a polymer based Kapton (supplier: Cole-Parmer) film is used to create an insulation between human skin and FTEG.
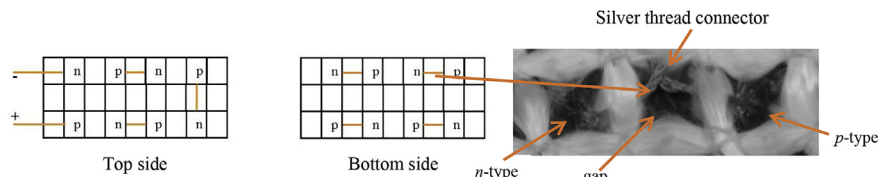
3.2. FTEG fabrication steps

Fig. 3 illustrates a step-by-step procedure to fabricate the FTEG prototypes. A flexible substrate is prepared using the polyester fabric with holes in it. The polyester fabric substrate hole is created manually with a hole size of 5 mm (±0.2 mm). The dimension of each hole is 5 × 5 mm², whereas the thickness is approximately 2.5 mm for prototype A and 1.4 mm for prototype B. A 5 mm gap is maintained between two consecutive holes as shown in Fig. 3(a). A hand sewing process is performed with a silver thread to connect holes which will be filled with n-type and p-type TE materials paste. Schematic diagrams of the top and the bottom views of connection between n-type and p-type holes for TE materials are shown in Fig. 3(b). Initially to make the printable paste, 80–82 wt% of n-type and 80–82 wt% of p-type TE materials powder are mixed manually with 18–20 wt% of Durabond-950 binder powder. Next, 18–20 wt% of Durabond-950 binder liquid is mixed with the composite mixer of TE materials and binder powder to make the printable paste (see Fig. 3(c)). The holes of the fabric substrate are then filled alternatively with prepared n-type and p-type paste (see Fig. 3(d)). The fabric substrate, filled with n-type and p-type paste, is kept at the room temperature for 24 h for initial curing. Subsequent curing is performed in a furnace chamber at 100 °C for 2 h (see Fig. 3(e)). After curing at 100 °C, it is recommended to cure the FTEG further at a higher temperature of 200–250 °C for 2 h to get good material bonding [30]. However, the developed FTEG prototypes are cured further at 160 °C for 2 h to avoid damaging the silver connective thread. Lastly, a Kapton film is attached to one side of the FTEGs which will be attached to the human skin (see Fig. 3(f)).

Fig. 4 shows two images of the fabricated FTEG prototypes.

(a)   (b)

Fig. 2. (a) Schematic presentation of the FTEG designed for the human body. (b) Bending and twisting characteristics of the FTEG.

(a) Preparing the polyester fabric as a substrate for FTEG

(b) Connection between n-type and p-type holes using silver thread for TE legs
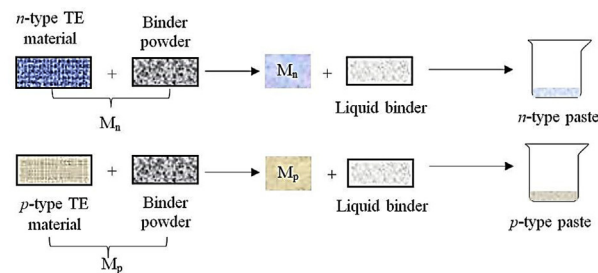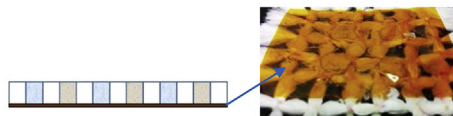

(c) Preparation of TE materials pastes using binder powder and liquid

(d) Fill up the holes with liquid paste with a dispenser (manually)
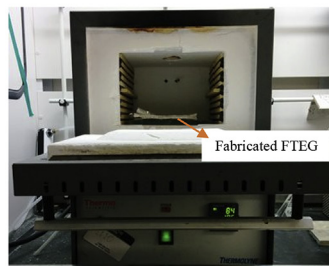
(e) Curing inside the furnace chamber

(f) Attached polyimide film at the bottom side of the fabricated FTEG

Fig. 3. (a)–(f) Fabrication steps for current fabricated FTEG prototypes using dispenser printing method.

Initial observation shows that the prototype has excellent bonding between the n-type and the p-type TE materials, binder material and the fabric substrate. Moreover, the fabricated prototypes are very flexible, twistable, and bendable.

4. Characteristics of the FTEG prototypes

The characteristics of the fabricated FTEG prototypes include: geometric and material characteristics of TE legs, theoretical
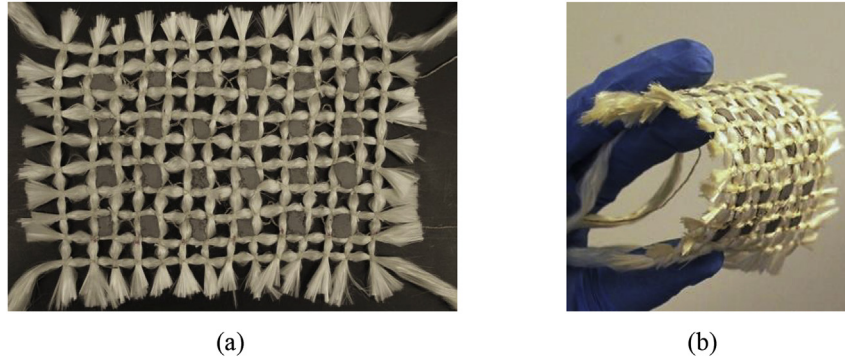
Fig. 4. (a) Fabricated FTEG prototype. (b) Bending of the FTEG prototype.

analysis of temperature distribution profile, output voltage and power, and microscopic structure of TE legs. Table 1 lists the geometric characteristics of the two fabricated prototypes (average size was considered for all dimensions) with the main difference being the thickness of the prototypes. The dimensions were measured by electronic caliper (supplier: Mastercraft) which had an accuracy of ±0.002 mm.

Fig. 5 shows the fabricated TE materials (n-type and p-type legs) properties (i.e., Seebeck coefficient, electrical resistivity, and thermal conductivity). These properties were measured at the CanmetMATERIALS Laboratory of the Natural Resources Canada at Hamilton, Canada. ZEM-3 equipment (supplier: Ulvac, Inc.) was used to measure the Seebeck coefficient and electrical resistivity while LF457 equipment (supplier: Netzsch, Inc.) was used to measure the thermal diffusivity of fabricated TE legs. The specific heat capacity of prepared TE legs was measured based on the hot disk method using TPS 500 (supplier: Thermtest, Inc.). Additionally, the density of the sample was measured based on the Archimedes' principle by MDS-300 (supplier: Alfa Mirage). The Seebeck coefficient and thermal conductivity of both n-type and p-type materials, and electrical resistivity of n-type material increase whereas electrical resistivity of p-type material decreases with increasing temperature. The properties of the fabricated n-type and p-type TE legs are extrapolated from Fig. 5 for subsequent theoretical analysis of designed FTEGs.

Fig. 6 shows numerical thermal fields and heat flow lines inside the TE legs generated using the FlexPDE software. The constant temperature (T_{Hs} and T_{Cs}) at the hot and cold surface of the TE legs and adiabatic process were considered for this numerical simulation of the temperature distribution profile. The hot surface temperature of the TE element was set relatively close to the human skin temperature assuming the very good contact between the skin and the FTEG. The simulated result shows that the temperature difference between two surfaces (ΔT_{TEG}) of the TE leg is around 0.3 °C (T_{Hs} = 31.9 °C and T_{Cs} = 31.6 °C) at ΔT = 10 °C between hot side (T_H = 32 °C, skin temperature varies from 32 to 35 °C [31]) and
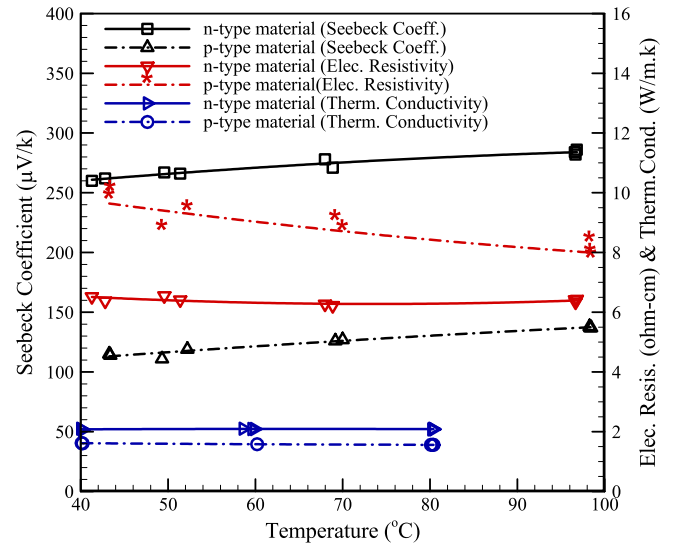

Fig. 5. Seebeck coefficient, electrical resistivity, and thermal conductivity of the fabricated TE legs.
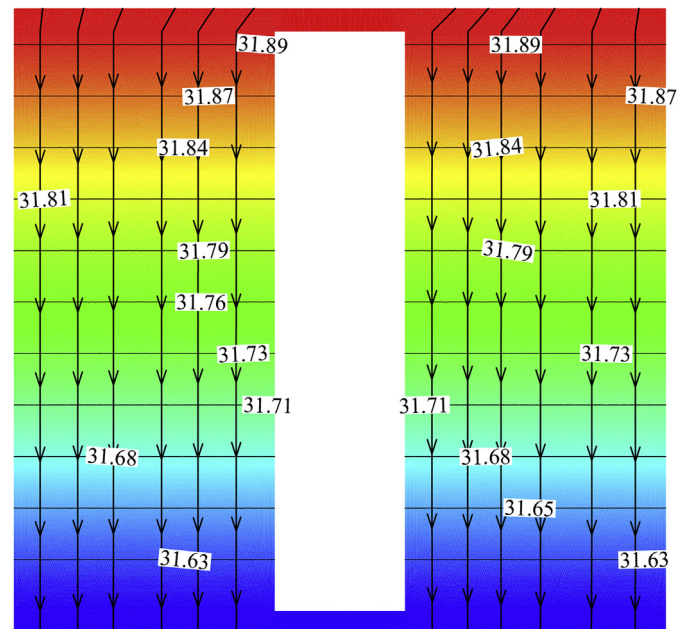

Fig. 6. Temperature profile of one pair of TE legs in the FTEG with heat flow.

Table 1
Characteristics of the fabricated FTEG prototypes.

Description	Prototype A	Prototype B
Size of single leg ($a \times b \times l$)	$5 \times 5 \times 2.5$ mm^3	$5 \times 5 \times 1.4$ mm^3
Size of the fabricated module	95×65 mm^2	65×50 mm^2
Thickness or height of TE leg (l)	2.5 mm	1.4 mm
Gap between two legs	5 mm	5 mm
Number of thermoelectric pairs	12	12
Initial measured resistance (R_{in})	272 kΩ	135 kΩ

surrounding temperature (assuming $T_C = 22$ °C). Due to this low-temperature difference, the power output becomes lower than expected.

Applying the method proposed in Refs. [32–34], voltage and power output of the fabricated FTEG prototypes were calculated analytically using the fabricated TE materials properties. One dimensional heat transfer equations (see Eqs. (4)–(10) below), applicable to the FTEG, was solved to calculate the voltage and power output with respect to temperature difference and load current [32–34]. The power output of FTEG prototype can be calculated as:

$$P = n\left(\dot{Q}_H - \dot{Q}_C\right) \tag{4}$$

where, P, n,$\dot{Q}_H$, and $\dot{Q}_C$ are the output power, number of TE pairs, the rate of heat entering to the hot side of the TE system, and the rate of heat leaving from the cold side of the TE system, respectively. $\dot{Q}_H$ and $\dot{Q}_C$ can be expressed as:

$$\dot{Q}_H = \alpha I_L T_{Hs} + K(T_{Hs} - T_{Cs}) - 0.5 I_L^2 R_{in} \tag{5}$$

$$\dot{Q}_C = \alpha I_L T_{Cs} + K(T_{Hs} - T_{Cs}) + 0.5 I_L^2 R_{in} \tag{6}$$

where, α ($= \alpha_n + \alpha_p$) is the Seebeck coefficient of the TE legs, I_L is the electrical load current, T_{Hs} is the hot surface temperature, T_{Cs} is the cold surface temperature, K is the thermal conductance, and R_{in} is the internal resistance of the FTEG prototype. If the temperatures are not constant then the energy balance equations between heat source and sink to TEG can be expressed as [32–34]:

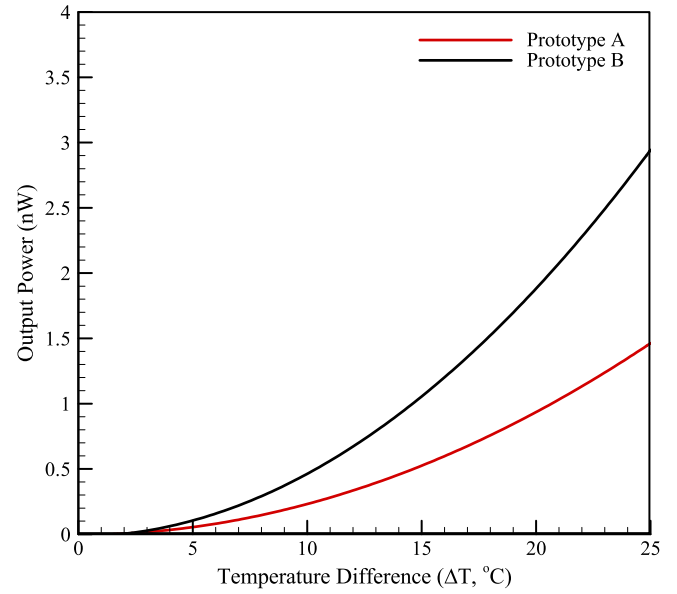$$\dot{Q}_H = h_1 A_1 (T_H - T_{Hs}) = \left[\alpha T_{Hs} I + K(T_{Hs} - T_{Cs}) - 0.5 I^2 R_{in}\right] \tag{7}$$

$$\dot{Q}_C = h_2 A_2 (T_{Cs} - T_C) = \left[\alpha T_{Hs} I + K(T_{Hs} - T_{Cs}) + 0.5 I^2 R_{in}\right] \tag{8}$$

where, $h_1 A_1$ is the heat conductance of the hot side where h_1 is heat transfer coefficient and A_1 is hot side heat transfer surface area of the TEG. Similarly $h_2 A_2$ is the heat conductance of the cold side where h_2 is heat transfer coefficient and A_2 is cold side heat transfer surface area of the TEG. Now, solving Eqs. (7) and (8), the final expression for T_{Hs} and T_{Cs} are given as:
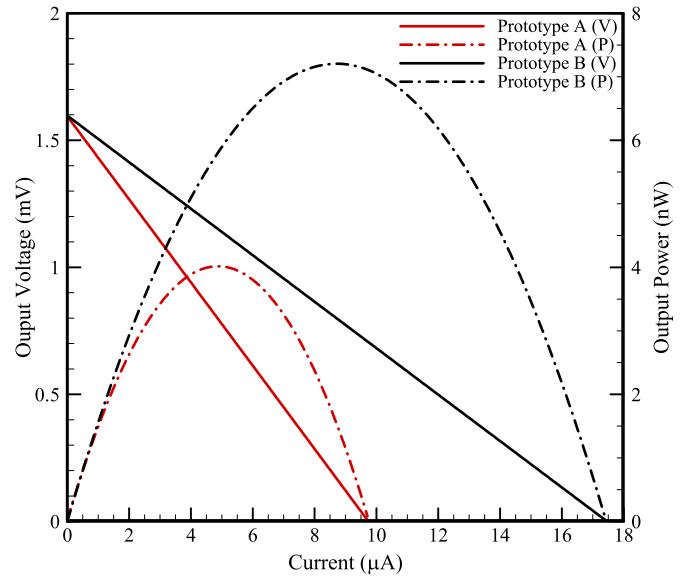
$$T_{Hs} = \frac{(K - \alpha I + h_2 A_2)(0.5 I^2 R_{in} + h_1 A_1 T_H) + K(0.5 I^2 R_{in} + h_2 A_2 T_C)}{(h_1 A_1 + K + \alpha I)(K - \alpha I + h_2 A_2) - K^2} \tag{9}$$

$$T_{Cs} = -\frac{K(-0.5 I^2 R_{in} - h_1 A_1 T_H) + (-h_1 A_1 - K - \alpha I)(0.5 I^2 R_{in} + h_2 A_2 T_C)}{(h_1 A_1 + K + \alpha I)(K - \alpha I + h_2 A_2) - K^2} \tag{10}$$

(a)

(b)

Fig. 7. Analytical results of fabricated FTEGs. (a) Output power against temperature difference. (b) Output voltage and power with respect to current.

Fig. 7 shows the analytical results of the fabricated FTEGs based on Eqs. (4)–(10). In Fig. 7(a), the power output of both prototypes is plotted as a function of temperature difference. The plot shows that the power output increases non-linearly as temperature difference increases from 0 °C to 25 °C. During analysis, hot and cold side surface area were considered 25 mm². Heat transfer coefficients

($h = 12.16$ Wm⁻²K⁻¹) for hot and cold surfaces of TE legs were calculated based on Ref. [35]. The Seebeck coefficient was considered from Fig. 5. Moreover, the plot also shows that power output of the prototype A remains lower than the prototype B because of higher internal resistance. Internal resistance is affected by the thickness of TE leg which is higher for the prototype A than the prototype B. Fig. 7(b) shows the voltage and power output as a

function of current when the temperature difference is 10 °C. Fig. 7(b) also shows that voltage output of the prototypes decreases linearly with increasing current flow.

The power output curve shows the rise in output power with the rise in electric current. However, after a certain rise in electric current, power output decreases due to the dominance of the irreversible Joule effect. Equations (5) and (6) present the heat input to and heat output from the TE system. Each equation has three terms: (i) Peltier heat (first term), (ii) Fourier heat conduction (second term), and (iii) heat generation or Joule heat (third term). Substituting Eqs. (5) and (6) into Eq. (4), the power output P can be expressed as $n\alpha I_L(T_{Hs} - T_{Cs}) - nI_L^2 R_{in}$. For given number of modules (n), constant temperature difference ($T_{Hs}-T_{Cs}$), and known properties (α and R_{in}) the magnitude of power output depends on the produced electric current. The Peltier power generation term is always positive and varies linearly with the current. However, the heat generation term (i.e. $nI_L^2 R_{in}$), which varies quadratically with current, possess a negative effect on the net power generation and varies. Therefore, power generation is zero when current is zero and in case of $n\alpha I_L(T_{Hs} - T_{Cs}) = nI_L^2 R_{in}$ which can be observed from Fig. 7(b). However, between these two limiting cases of zero power generation there is an optimum value of electric current ($=\alpha\Delta T/R_{in}$) which maximizes the net power output. This optimum value of current depends on α, R_{in}, and ΔT. Any current larger than this optimum value causes the reduction of the net power output from its peak value. The peak values in Fig. 7(b) show that the power output is maximum at one specific electric current value for a given temperature difference condition provided that the geometric and thermophysical properties are constant.

The scanning electronic microscopy (SEM) method was used to visualize the microstructure of the freshly fractured surface of TE legs as well as the connection between the silver thread and the substrate to the TE legs. The microstructure was obtained by using Hitachi S-570 Scanning Electron Microscope (supplier: Hitachi High-Technologies, Tokyo, Japan). Fig. 8 illustrates different SEM images of the fabricated FTEG legs. Fig. 8 (a) and 8 (c) provide SEM surface images of *p*-type and *n*-type legs, respectively, which indicate that the surface is not very smooth at a magnification of 15 μm. In some space bonding of TE materials with the binder is quite good whereas some portion is not bonded well with each other. Fig. 8 (b) and 8 (d) provide a cross-sectional view of freshly fractured *p*-type and *n*-type legs, respectively, at a magnification of 30 μm. These cross-sectional SEM images show that the grains are randomly oriented and there are some void spaces between the solid structures. A possible reason for this may be the lack of additional pressure applied to the substrate during the fabrication process. Fig. 8 (e) and 8 (f) show the bonding condition between TE materials and the substrate, and connection of silver thread (circled area) to the TE legs, respectively. From Fig. 8, it can be said that the electrical resistivity is very high due to some void spaces. Therefore, the overall current output decreases and subsequently power output decreases.

5. Experimental tests and results

Experimental tests were performed on the two fabricated FTEG
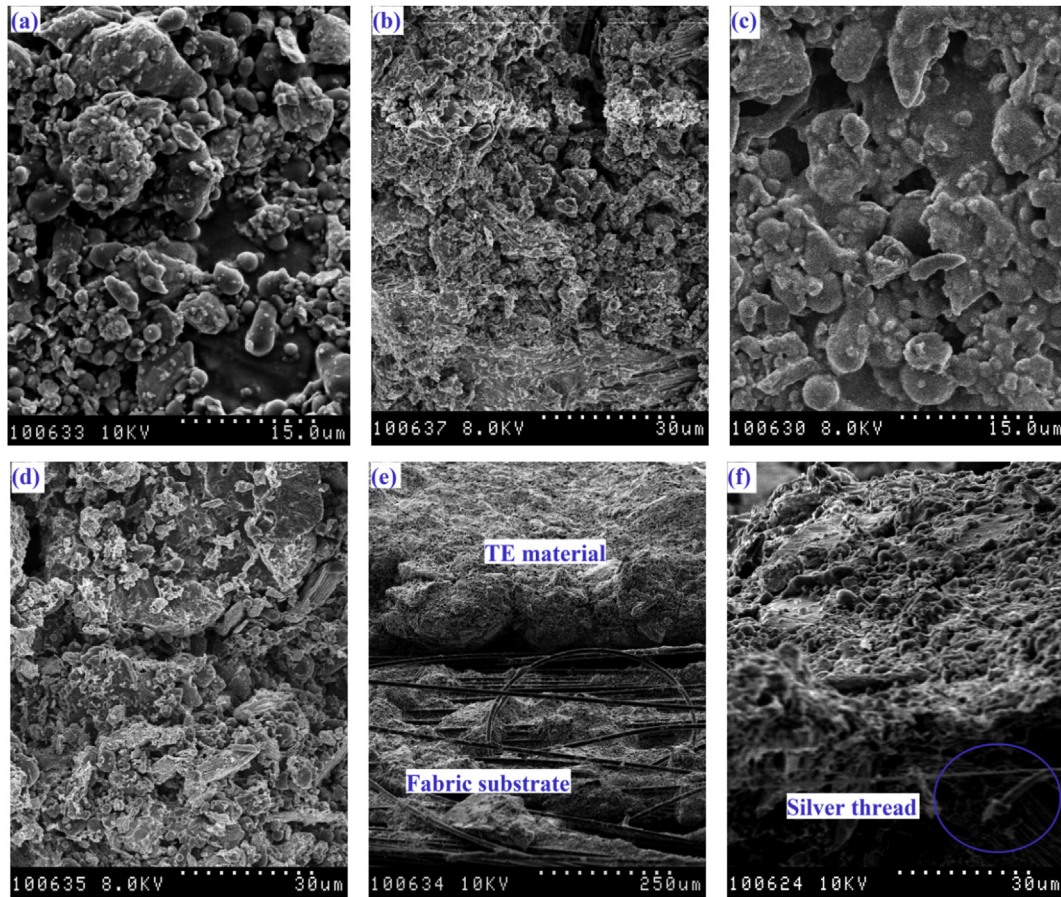
Fig. 8. (a) and (c) provide SEM surface images of *p*-type and *n*-type legs, respectively. (b) and (d) provide a cross-sectional view of freshly fractured *p*-type and *n*-type legs, respectively. (e) and (f) show the bonding condition between TE materials and the substrate.
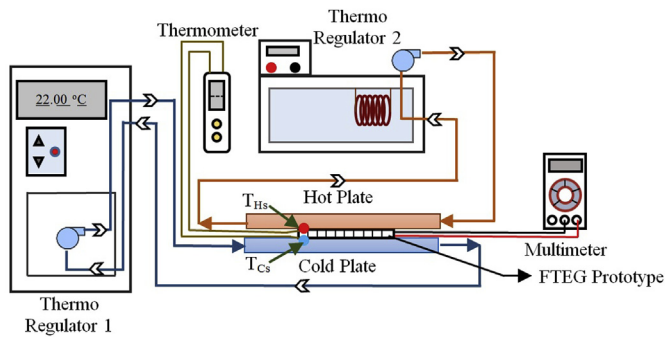
Fig. 9. Schematic diagram of the experimental set-up.

prototypes to measure output voltage and power in a controlled lab environment. Additionally, the performance of the FTEGs was tested by attaching them to the arm of the human body while under different body conditions (e.g., standing, sitting, walking, and running).

5.1. Lab test

Fig. 9 illustrates the schematic diagram of the experimental setup developed to measure the voltage and current output of the fabricated FTEG prototypes. The experimental setup includes two thermo-regulators to create a controlled temperature environment, two heat exchangers, thermometer with a K-type thermocouple, and a multimeter. Cold temperature was maintained by one thermo-regulator (supplier: Cole-Parmer; model number: polystat CR250WU re-circulator) with a temperature range from 0 °C to 80 °C and temperature stability of ± 0.1 °C (Thermo-regulator 1 in Fig. 9). The high temperature was maintained by a second thermo-regulator (supplier: Omega; model number: HCTB 3020) with a working temperature range of ambient to 120 °C and temperature stability of ± 0.1 °C (Thermo-regulator 2 in Fig. 9). Thermo-regulator 1 was used to supply water at low temperatures to a plate and tube heat exchanger while thermo-regulator 2 supplied hot water to a

second plate and tube heat exchanger (supplier: Lytron Inc.). The hot-side heat exchanger was used to mimic the human body with a temperature of 32 °C while the cold-side heat exchanger was used to mimic the ambient temperature condition ranging from 9.5 °C to 31 °C. Temperatures at the hot and cold surfaces of the FTEG were monitored using the Omega-HH374 thermometer. A digital multimeter (supplier: Amprobe; model: 37XR-A) was used to measure the electric voltage and the current generated by the prototypes.

Fig. 10 illustrates the variation in the open circuit output voltages generated by the FTEG prototypes with respect to time. Study of such transient behavior is significant to identify the performance
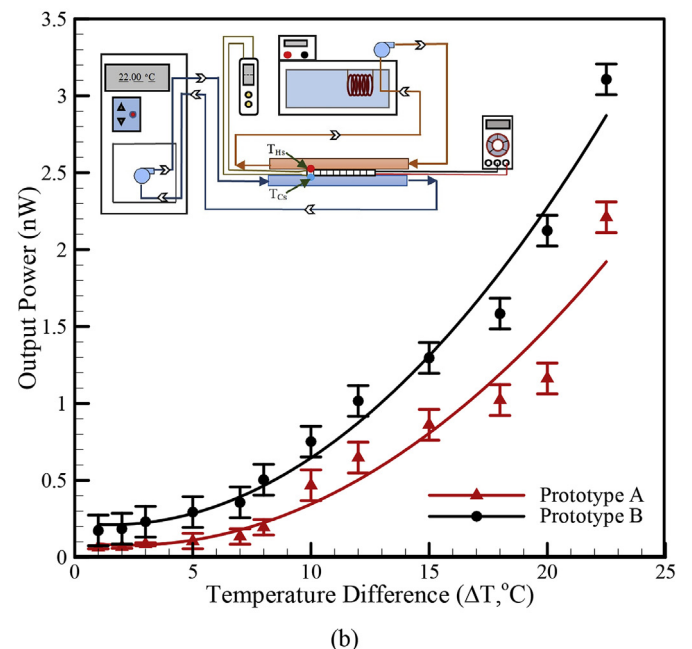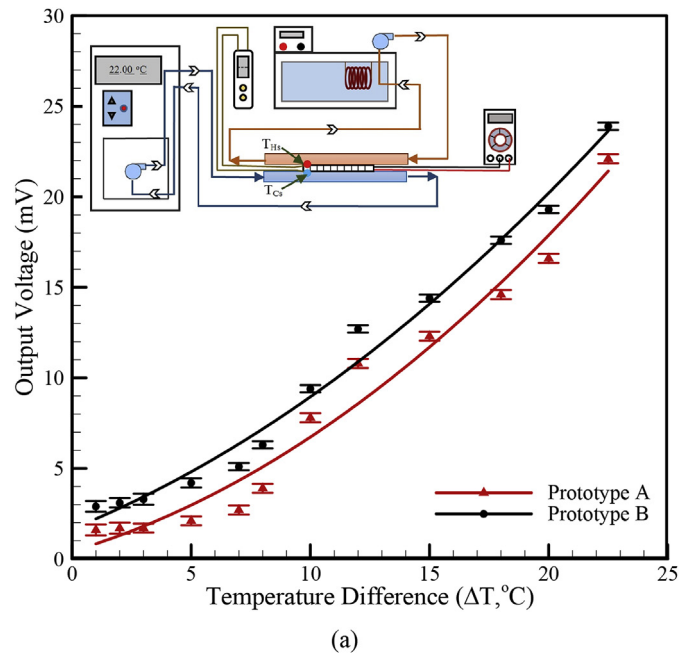

(a)

(b)

Fig. 11. (a) Open circuit voltage output and (b) power output from experimental tests with respect to constant temperature difference between two surfaces for two fabricated FTEGs (Note: symbol indicates the experimental data and the solid lines indicate the best fir curve).
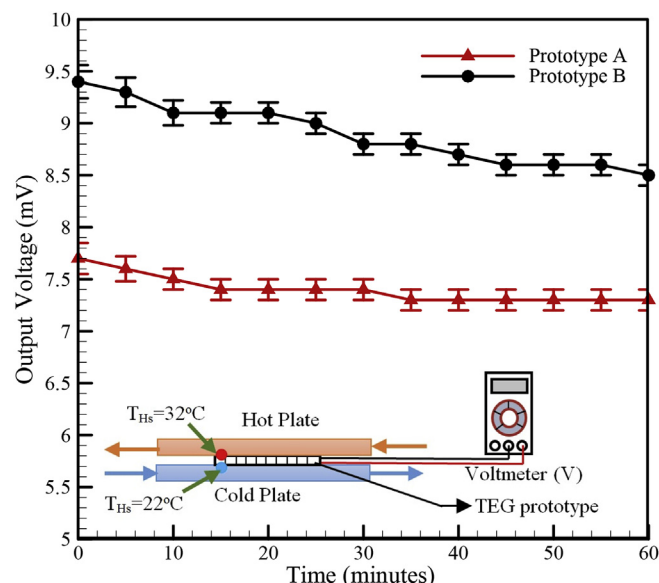

Fig. 10. Open circuit voltage output of FTEG prototypes from constant temperature experimental test with respect to time at a temperature difference of 10 °C.

characteristics of FTEG prototypes over the duration of use. This test was carried out multiple times inside the lab environment by applying a constant temperature difference (i.e., $\Delta T_{TEG} = 10$ °C) between the hot surface ($T_{Hs} = 32$ °C) and cold surface ($T_{Cs} = 22$ °C) of the FTEG systems. Fig. 10 illustrates that the voltage output for both prototypes decrease with increasing time and reached a steady-state value after a certain time. The error bar represents the range of the open circuit output voltages generated during each tests by prototype A and prototype B. At the beginning, both prototypes generate their maximum voltage due to the largest temperature difference between the two surfaces. However, as time advances, the irreversible internal heat transfer mechanism raises the cold surface temperature and consequently reduces the temperature difference between two surfaces. Therefore, the output voltage reduces as time advances. The low thermal resistance and low heat dissipation rate from the cold surface can be the reasons for degrading the voltage over the course of time.

Fig. 11(a) and (b) show the open circuit voltage and power output (calculated using Eq. (2)) of the FTEGs as a function of temperature difference (i.e., cold surface temperature varies from 9.5 °C to 31 °C and the hot surface is fixed at 32 °C). The data were recorded when the output voltage became stable (approximately 10–15 min after of each temperature difference was applied). Results obtained from both prototypes are presented in Fig. 11 for a comparison purpose and indicate that the trend in the voltage and power output remain similar for both prototypes. Prototype B, however, generated more voltage and more power than prototype A at a given temperature difference. This can be attributed to the lower thickness of prototype B compared to prototype A. The internal resistance ($R_{in} = \rho l/A$) of the TE legs decreases with decreasing thickness (l) and, according to Eq. (3), power output will be increased. Therefore, prototype B can generate more power than prototype A. Table 2 shows the maximum open circuit output voltage and power of the prototypes at open circuit condition at $\Delta T_{TEG} = 5$ °C and $\Delta T_{TEG} = 22.5$ °C.

The output voltage of the fabricated FTEG prototypes is suitable to power a range of portable electronic devices (e.g., active RFID locators, wireless heart rate monitors, wireless pedometers, wireless oximeter, digital watches, etc.) which require very small power (<mW) [36]. However, the lower current output of FTEG prototypes results in a lower power output. Potential causes for lower power output are discussed:

- The p-type and n-type legs are surrounded by polyester fabric which is not a good thermal insulator. Therefore, heat loss occurs from the side wall surfaces of the FTEG system to the surrounding environment through the polyester fabric. Such heat loss lowers the direct energy conversion from body heat to electricity and consequently reduces the efficiency of the FTEG [33].
- The relatively higher thickness of the FTEG prototype compared to the prototypes reported in the literature results in a higher internal electrical resistance, which is responsible for lower power output.
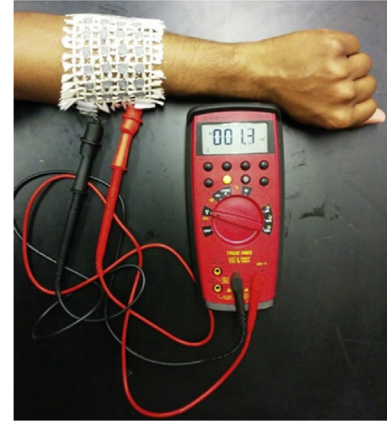

Fig. 12. Fabricated FTEG attached to human arm.

5.2. Test on human body

The fabricated FTEG prototypes were attached to a human arm and tested for the power output capability (see Fig. 12). Table 3 presents the open circuit voltage and power output from the prototypes at different test conditions. Both prototypes harvest maximum voltage and power at maximum temperature difference which is in the cold environment. Prototypes generate maximum power during running condition compared to walking condition due to the temperature drop at the outer surface of the FTEGs because of increasing rate of heat convection. Moreover, FTEGs generate minimum voltage and power at sitting and standing condition compared to other conditions.

5.3. Uncertainty analysis of the experimental results

The experimental results have different uncertainties pertaining to the test equipment. It is clear from experimental results that the voltage and power output of the fabricated FTEGs are highly influenced by the temperature difference between the surfaces of the FTEG. Therefore, thermometer and multi-meter were considered in order to determine the uncertainty of the experimental results of FTEGs. The uncertainty analysis was accomplished using the root-sum-squared (RSS) method [37]. The uncertainty of the statistical data analysis was assumed 95% confidence interval for each calculated variable. Table 4 represents the uncertainty of the measured variables by thermometer and multi-meter that were used in the experiment. The analysis was completed for a specific temperature difference i.e., $\Delta T_{TEG} = 10$ °C for prototype A.

Using the value of V and I from Table 4, the relative uncertainty of the harvested power for the currently fabricated FTEGs can be calculated by:

$$U_p = \sqrt{\left(\frac{U_V}{x_V}\right)^2 + \left(\frac{U_I}{x_I}\right)^2} \tag{11}$$

Table 2
Harvested open circuit voltage and power from the experimental tests of prototype A and prototype B.

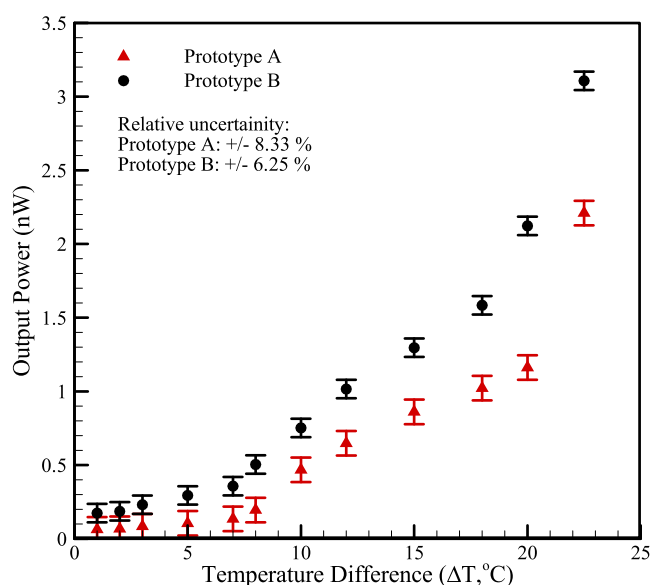| Prototype	Hot surface temperature (°C)	Cold surface temperature (°C)	Voltage (mV)	Power (nW)
A	32	27	2.1	0.105
	32	9.5	22.1	2.21
B	32	27	4.2	0.294
	32	9.5	23.9	3.107

Table 3
Open circuit voltage and power output at different test conditions of human body (arm).

Test condition	Temperature difference between body and ambient (°C)	Temperature difference between the two surfaces of the FTEG (°C)	Prototype	Output voltage (mV)	Output power (nW)
Sitting inside the lab, FTEG is horizontally placed with respect to ground	10.9	2.3	A	1.3	0.026
			B	2.1	0.063
Standing inside the lab, FTEG is vertically placed with respect to ground	10.9	2.3	A	1.2	0.024
			B	1.9	0.057
Walking	11.4	2.4	A	1.6	0.032
			B	2.4	0.072
Running	11.9	2.9	A	1.7	0.034
			B	2.6	0.078
Cold environment	32.9	11.9	A	9.1	0.182
			B	11.3	0.339

Table 4
Uncertainty analysis of the experimental results of prototype A for $\Delta T_{TEG} = 10$ °C.

Sensors and equipment	Accuracy, U_C	Measured value (x)	Relative uncertainty (U_C/x)
Thermometer	±0.1% [°C]	$T_{Hs} = 32$ °C	±0.0031%
		$T_{Cs} = 22$ °C	±0.0045%
Multi-meter	±0.1% [mV]	$V = 7.8$ mV	±0.013%
	±0.5% [μA]	$I = 0.06$ μA	±8.33%
	±0.5% [kΩ]	$R = 272$ kΩ	±0.0018%

Fig. 13. Uncertainty analysis of experimental power output for prototype A and prototype B.

where, U_p is the relative uncertainty of output power, U_V and U_I are the accuracy of the measuring instrument for voltage and current, respectively, and x_V and x_I are the measured value of voltage and current, respectively of the system. According to Eq. (11), the relative uncertainty of the power output of the prototype A and prototype B were around ± 8.33% and ±6.25%, respectively, at $\Delta T_{TEG} = 10$ °C. Fig. 13 presents the relative uncertainty of the power generation by FTEG prototype A and prototype B at temperature difference ranging from 0 °C to 25 °C.

6. Conclusion

In this research work, a complete manual fabrication process for a FTEG is presented. The FTEG can be used as an alternative power source for self-powered portable electronic devices. The FTEG prototypes were fabricated with a simple dispenser printing method using a polyester based, high heat resistive fabric and using n-type $(0.98Bi,0.02Sb)_2(0.9Te,0.1Se)_3$ and p-type $(0.25Bi,0.75Sb)_2(0.95Te,0.05Se)_3$ TE materials. The prototypes had high flexibility, durability, and were well suited for human body applications.

The fabricated prototypes were characterized in terms of material properties and structure, one-dimensional theoretical analysis, and experimental results. SEM images were also obtained to determine the surface and cross-sectional structures of the fabricated n-type and p-type TE legs. The maximum open circuit voltage and power output of prototype A ($5 \times 5 \times 2.5$ mm^3) and prototype B ($5 \times 5 \times 1.4$ mm^3) were 22.1 mV and 2.21 nW, and 23.9 mV and 3.107 nW, respectively, at 22.5 °C temperature difference. Moreover, the power output and voltage generation showed similar experimental and theoretical trends (according to Figs. 7(a) and 11(b)). Uncertainty analysis of fabricated prototypes was also performed. The fabricated prototypes were tested under different body conditions at different temperatures to assess the variation of the open circuit voltage and power output under real environment conditions.

Future work will be focused on the fabrication process using a thinner substrate with automated controlled dispenser machine so that the fabrication mechanism can be more precise. Moreover, different TE materials, proper insulation, printed circuit board, and optimization of geometrical structures can be investigated for the further developments in the field of FTEG.

References

[1] Torfs T, Leonov V, Van Hoof C, Gyselinckx B. Body-heat powered autonomous pulse oximeter. Proc IEEE Sensors 2006:427—30.

[2] Lay-Ekuakille A, Vendramin G, Trotta A, Mazzotta G. Thermoelectric generator design based on power from body heat for biomedical autonomous devices. In: 2009 IEEE Int Work Med Meas Appl MeMeA; 2009. p. 1—4.

[3] Wearable thermoelectric generator could extend your smartwatch's battery life. KAIST; 2014. http://www.gizmag.com/wearable-thermoelectric-generator/31617.

[4] Chye WC, Dahari Z, Sidek O, Miskam MA. Electromagnetic micro power generator-A comprehensive survey. In: 2010 IEEE Symp Ind Electron Appl; 2010. p. 376—82. http://dx.doi.org/10.1109/ISIEA.2010.5679438.

[5] Dunhama MT, Barako MT, LeBlanc S, Asheghi M, Chen B, Goodson KE. Power density optimization for micro thermoelectric generators. Energy 2015;93: 2006—17.

[6] Tran V, Tran N, Yu S, Park Y, Choi W. Design of a nonisolated fuel cell boost charger for lithium polymer batteries with a low output ripple. IEEE Trans Energy Convers 2015;30(2):605—14.

[7] Siddique ARM, Mahmud S, Heyst BV. A comprehensive review on vibration based micro power generators using electromagnetic and piezoelectric transducer mechanisms. Energy Convers Manage 2015;106:728—47.

[8] Gou X, Yang S, Xiao H, Ou Q. A dynamic model for thermoelectric generator applied in waste heat recovery. Energy 2013;52:201e9.

[9] Arnold DP. Review of microscale magnetic power generation. IEEE Trans Magn 2007;43:3940—51.

[10] Li G, Qian S, Lee H, Hwang Y, Radermacher R. Experimental investigation of energy and exergy performance of short term adsorption heat storage for residential application. Energy 2014;65:675e91.

[11] Georgopoulou Chariklia A, Dimopoulos George G, Nikolaos MPK. A modular dynamic mathematical model of thermoelectric elements for marine applications. Energy 2013;94:13—28.

[12] We JH, Kim SJ, Cho BJ. Hybrid composite of screen-printed inorganic thermoelectric film and organic conducting polymer for flexible thermoelectric power generator. Energy 2014;73:506—12.

[13] Favarel C, Bedecarrats J-P, Kousksou T, Champier D. Numerical optimization of the occupancy rate of thermoelectric generators to produce the highest electrical power. Energy 2014;68:104e16.

[14] Qu W, Plötner M, Fischer W-J. Microfabrication of thermoelectric generators on flexible foil substrates as a power source for autonomous microsystems. J Micromechanics Microengineering 2001;11:146—52.

[15] Kim MK, Kim MS, Jo SE, Kim YJ. Flexible thermoelectric generator for human body heat energy harvesting. Electron Lett 2012;48:1015—7. http://dx.doi.org/10.1049/el.2012.1566.

[16] Yadav A, Pipe KP, Shtein M. Fiber-based flexible thermoelectric power generator. J Power Sources 2008;175:909—13.

[17] Hasebe S, Ogawa J, Toriyama T, Sugiyama S, Ueno H, Itoigawa K. Design and fabrication of flexible thermopile for power generation. In: MHS2003 Proc 2003 Int Symp micromechatronics Hum Sci (IEEE Cat No03TH8717); 2003.

[18] Schwyter E, Glatz W, Durrer L, Hierold C. Flexible micro thermoelectric generator based on electroplated Bi$_{2+x}$Te$_{3-x}$. In: DTIP MEMS MOEMS - Symp Des Test, Integr Packag MEMS/MOEMS; 2008. p. 46—8. http://dx.doi.org/10.1109/DTIP.2008.4752949.

[19] Navone C, Soulier M, Plissonnier M, Seiler AL. Development of (Bi,Sb)$_2$(Te,Se)$_3$-based thermoelectric modules by a screen-printing process. J Electron Mater 2010;39:1755—9. http://dx.doi.org/10.1007/s11664-010-1187-3.

[20] Francioso L, De Pascali C, Farella I, Martucci C, Cretì P, Siciliano P, et al. Flexible thermoelectric generator for wearable biometric sensors. Proc IEEE Sensors 2010:747—50.

[21] Suemori K, Hoshino S, Kamata T. Flexible and lightweight thermoelectric generators composed of carbon nanotube—polystyrene composites printed on film substrate. Appl Phys Lett 2013;103:1—4.

[22] Madan D, Wang Z, Chen A, Wright PK, Evans JW. High-performance dispenser printed MA p-type Bi$_{0.5}$Sb$_{1.5}$Te$_3$ flexible thermoelectric generators for powering wireless sensor networks. ACS Appl Mater Interfaces 2013;5:11872—6. http://dx.doi.org/10.1021/am403568t.

[23] Kim MK, Kim M-S, Lee S, Kim C, Kim Y-J. Wearable thermoelectric generator for harvesting human body heat energy. Smart Mater Struct 2014;23:105002. http://dx.doi.org/10.1088/0964-1726/23/10/105002.

[24] Kim MK, Kim MS, Jo SE, Kim HL, Lee SM, Kim YJ. Wearable thermoelectric generator for human clothing applications. In: 2013 transducers eurosensors XXVII 17th Int. Conf. Solid-state sensors, actuators microsystems, TRANS-DUCERS EUROSENSORS; 2013. p. 1376—9.

[25] Lee HB, We JH, Yang HJ, Kim K, Choi KC, Cho BJ. Thermoelectric properties of screen-printed ZnSb film. Thin Solid Films 2011;519:5441—3.

[26] Yono T, Suzuki RO, Ono K. Conversion of unused heat energy to electricity by means of thermoelectric generation in condenser. IEEE Trans Energy Convers 2003;18:330—4. http://dx.doi.org/10.1109/TEC.2003.811721.

[27] Li G, Hwang Y, Radermacher R, Chun H-H. Review of cold storage materials for subzero applications. Energy 2013;51:1e17.

[28] Hamid Elsheikh M, Shnawah DA, Sabri MFM, Said SBM, Haji Hassan M, Ali Bashir MB, et al. A review on thermoelectric renewable energy: principle parameters that affect their performance. Renew Sustain Energy Rev 2014;30: 337—55.

[29] Jang B, Han S, Kim J-Y. Optimal design for micro-thermoelectric generators using finite element analysis. Microelectron Eng 2011;88:775—8.

[30] Material data Sheet Durabond-950, Supplier- iS-Connect. 2015. http://www.is-connect.com/ [accessed 05.10.15].

[31] Freitas Jr RA. Nanomedicine. volume I: basic capabilities, landes bioscience, (8.4.1.1 thermography of the Human Body). Georgetown: Texas; 1999.

[32] Alomair M, Alomair Y, Mahmud S, Abdullah HA. Theoretical and experimental investigations of solar-thermoelectric air-conditioning system for remote applications. J Therm Sci Eng Appl 2015;7(2). 021013:1-10.

[33] Shen ZG, Wu SY, Xiao L, Yin G. Theoretical modeling of thermoelectric generator with particular emphasis on the effect of side surface heat transfer. Energy 2016;95:367—79.

[34] Chen L, Gong J, Sun F, Wu C. Effect of heat transfer on the performance of thermoelectric generators. Int J Therm Sci 2002;41:95—9.

[35] Arpaci VS, Selamet A, Kao S. Introduction to heat transfer: chapter 6-correlation for convection. Prentice Hall Inc; 2000. p. 312—7.

[36] Stark I. Converting body heat into reliable energy for powering physiological wireless sensors. In: Proc. 2nd Conf. Wirel. Heal. - WH '11. ACM Press; 2011. p. 1.

[37] Moffat RJ. Describing the uncertainties in experimental results. Exp Therm Fluid Sci 1988;1:3—17.